

A histidine residue and a tetranuclear cuprous-thiolate cluster dominate the copper loading landscape of a copper storage protein from *Streptomyces lividans*

Megan L. Straw, Michael A. Hough, Michael T. Wilson and Jonathan A.R. Worrall*

School of Biological Sciences, University of Essex, Wivenhoe Park, Colchester, CO4 3SQ,
U.K.

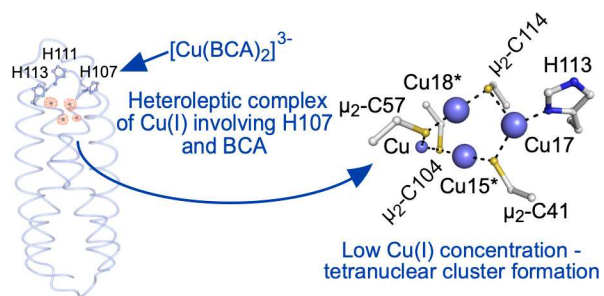
*Corresponding author: jworrall@essex.ac.uk

ABSTRACT

The chemical basis for protecting organisms against the toxic effect imposed by excess cuprous ions is to constrain this through high-affinity binding sites that employ cuprous-thiolate coordination chemistries. In bacteria, a family of cysteine rich four helix-bundle proteins utilise thiolate chemistry to bind up to 80 cuprous ions. These proteins have been termed copper storage proteins (Csp). The present study investigates cuprous ion loading to the Csp from *Streptomyces lividans* (*SlCsp*) using a combination of X-ray crystallography, site-directed mutagenesis and stopped-flow reaction kinetics with either aquatic cuprous ions or a chelating donor. We illustrate that at low cuprous ion concentrations, copper is loaded exclusively into an outer core region of *SlCsp* via one end of the four helix-bundle, facilitated by a set of three histidine residues. X-ray crystallography reveals the existence of polynuclear cuprous-thiolate clusters culminating in the assembly of a tetranuclear $[\text{Cu}_4(\mu_2\text{-S-Cys})_4(\text{N}^{\delta 1}\text{-His})]$ cluster in the outer core. As more cuprous ions are loaded, the cysteine lined inner core of *SlCsp* fills with cuprous ions but in a fluxional and dynamic manner with no evidence for the assembly of further intermediate polynuclear cuprous-thiolate clusters as observed in the outer core. Using site-directed mutagenesis a key role for His107 in the efficient loading of cuprous ions from a donor is established. A model of copper loading to *SlCsp* is proposed and discussed.

GRAPHICAL ABSTRACT

Warehousing cuprous copper: A histidine residue facilitates Cu(I) loading to a copper storage protein creating a Cu(I)-thiolate cluster before the inner core is loaded.



INTRODUCTION

Copper (Cu) is an essential micronutrient in aerobic organisms.^[1] The ability of Cu to cycle between the cupric and cuprous oxidation states is exploited by many proteins and enzymes that engage in specific biological processes such as electron-transfer, oxygen activation, oxygen reduction to water, and denitrification.^[2] Although essential, maintaining cellular Cu homeostasis, so as to prevent the detrimental effects associated with Cu overload is, amongst other factors, a pre-requisite for cell viability. Over recent years several theories have emerged as to how the cuprous form imparts its toxic effect.^[3] To balance the metabolic demands and safeguard against toxicity, organisms have evolved highly sophisticated homeostasis and resistance mechanisms in order to maintain the 'normal' cellular Cu supply to essential cuproenzymes, while detoxifying excess Cu.^[4] The chemical basis for safeguarding Cu(I) is to tightly constrain it through high-affinity sites in proteins and low molecular weight ligands employing Cu(I) thiolate chemistries.^[5] Moreover, bacteria have no known metabolic requirement for Cu in their cytoplasm, thus further reducing the possibility of detrimental effects. Therefore, the discovery of a protein family located in the cytoplasm of many bacteria with a high capacity to bind multiple Cu(I) ions has added a new layer of intrigue into the complexity of how bacteria handle, distribute and safeguard cytoplasmic Cu(I).^[5g, 6]

Copper storage proteins (Csp) were first identified in the soluble extracts from cells of the methanotrophic bacterium *Methylosinus trichosporium* OB3b grown under elevated Cu conditions.^[5g] A total of three Csp proteins were identified in *M. trichosporium* OB3b, with *MtCsp1* and *MtCsp2* possessing Tat signal sequences, consistent with their secretion to the periplasm.^[5g] A role for *MtCsp1/2* in storing Cu(I) for metalation of particulate methane monooxygenase has been suggested.^[5g, 6b, 7] *MtCsp3*, on the other hand, did not possess a signal sequence, implying that it occupies a cytosolic location.^[5g] *MtCsp1* and *MtCsp3* are structurally similar, comprising of a four helix-bundle that form a homotetramer assembly, with Cys residues in each four helix-bundle inwardly facing to create a solvent shielded core that can accommodate Cu(I) thiolate binding with affinities of 10^{17} M^{-1} .^[5g, 6a] *MtCsp1* has 13 Cys residues and can coordinate up to 13 Cu(I) ions per four helix-bundle (52 per homotetramer).^[5g] *MtCsp3*, on the other hand has 18 Cys residues, and can coordinate up to 19 Cu(I) ions (76 per homotetramer).^[6a] Thus, the cytosolic *MtCsp3* has a higher Cu(I) binding capacity than *MtCsp1/2*.

Csp3 members are now known to be taxonomically distributed amongst seven bacterial groups, including proteobacteria and terrabacteria.^[8] Structural studies of non-methanotrophic Csp3 members reveal structural homology with *MtCsp3*,^[6a, 8] but only the Csp3 from the Gram-

positive bacterium *Streptomyces lividans*, previously referred to as Ccsp (*SlCsp3* herein), has been structurally characterised with Cu(I) bound, revealing up to 20 Cu(I) ions can bind per four helix-bundle of *SlCsp3* (80 per homotetramer).^[8] In addition to the extra Cys residues lining the four helix-bundle core in Csp3s compared to *MtCsp1/2*, a set of three His residues are present at one end of the four helix-bundle, which together with nearby Cys residues also participate in Cu(I) coordination.^[6a, 8] The His end of the four helix-bundle is considered from structural insights to be the loading and leaving point for Cu(I), as access to the Cys core from the opposite end of the bundle is prevented by hydrophobic side chains.^[6a, 8] Further Cu(I) coordination arises from the O^{δ1} atom of an Asn residue (58 in *MtCsp3*)^[6a] and the O^{δ1} and O^{δ2} atoms of an Asp residue (61 in *SlCsp3*).^[8] The Asp and the Asn residues are highly conserved across Csp3 species and are structurally positioned to create a crossing point, dividing the Cu(I) ions participating in His/Cys coordination at the mouth of the Cys core and those coordinated solely through bis-cysteinate coordination in the Cys core.

To circumvent the potentially toxic effects of aqueous Cu(I) ions in the bacterial cytoplasm, Cu(I) is moved between sites in a defined manner. The accepted view of cellular Cu(I)-trafficking *i.e.* transfer of Cu(I) from a donor to an acceptor, is that it comprises of a ligand-substitution process at the inorganic center,^[9] a fundamental process of inorganic reaction mechanisms.^[10] In this manner a Cu(I)-bound donor (protein or low molecular weight ligand) associates with an acceptor, enabling intrusion into the donor coordination sphere of a ligand from the acceptor, ensuring that Cu(I) remains at all time coordinated between donor and acceptor and facilitating rapid Cu(I) exchange.^[5a, 9, 11] Therefore, for Csp3 members to act as a cytosolic Cu(I) store, cuprous ions will need to be delivered by a Cu(I) donor. At present the physiological donor to Csp3 is unknown.

Recent insights into Cu(I)-loading of *MtCsp3* have been obtained through X-ray crystallography studies.^[12] Structures determined at various Cu(I) to protein ratios reveal the existence of initial tetranuclear Cu(I)-thiolate clusters, [Cu₄(μ₂-S-Cys)₄], located in the Cys core (Cu sites 3 to 14) of the four helix-bundle.^[12] As more Cu(I) is loaded the tetranuclear clusters considered as ‘intermediates’ evolve into the final Cu(I) coordinated states.^[12] Thus, the formation of tetranuclear clusters is considered a driving force for acquisition and safe initial storage of Cu(I) by Csp3 members.^[6c, 12]

The present study investigates through a combination of X-ray crystallography, stopped-flow kinetics and site-directed mutagenesis the loading of Cu(I) to *SlCsp3*, a non-methanotrophic Csp3 member. Our data reveal that at low Cu(I) loadings, polynuclear Cu(I)

clusters form exclusively in the His entrance of the four helix-bundle. As more Cu(I) ions are loaded, Cu(I) sites become occupied to varying extents in the Cys core. Kinetic studies using the Cu(I) bicinchoninic acid complex ($[\text{Cu}(\text{BCA})_2]^{3-}$) as a Cu(I) nitrogen donor, reveals rapid uptake by *S/Csp3* of two Cu(I) ions within the first few seconds of the reaction time course, followed by additional slower phases. The role of the His residues lining one end of the four helix-bundle in Cu(I) loading have been determined, offering the first experimental kinetic evidence that Cu(I) loads at the His end. From these data, a model of Cu(I) binding to *S/Csp3* is proposed and discussed.

RESULTS

Definition of Cu(I) sites and their grouping within S/Csp3

From previous structural characterisation of Csp3 members, modes of Cu(I) binding within the protein have been discussed and defined.^[6a, 6c, 8] Prior to reporting the results from the present study, we briefly define Cu(I) sites, cores and coordination. For *S/Csp3* the positions of the 20 Cu(I) ions of the fully Cu(I)-loaded form are shown in Fig. 1A and can be subdivided into outer and inner cores (dashed red lines Fig. 1) that incorporate the Cu(I) sites, 1-14 (inner), and 15-20 (outer) (Fig. 1A).^[8] Within these two cores Cu(I) coordination can be divided into three groups based on differences in coordination environment.^[6c] In group I, Cu(I) ions are coordinated by two Cys thiolates on the same helix in a CXXXXC motif, in group II, by two Cys thiolates on different helices of the four helix-bundle and in group III, by Cys thiolates and other atoms e.g. $\text{N}^{\delta 1}$ or O^{δ} from His or Asp, respectively. The Cu(I) ions in *S/Csp3* assigned to each of these groups are reported in the legend to Fig. 4.

Polynuclear Cu(I) clusters form in the outer core at low Cu(I) loading

The X-ray structure of *S/Csp3* incubated with 5 Cu(I)-equivalents was found to contain 4 four helix-bundles in the asymmetric unit arranged in a similar manner to apo-*S/Csp3*.^[8] We refer to each of these four helix-bundles as monomers, *i.e.* monomer A, B, C and D. Anomalous electron-density map features were evident in each monomer, which were used, together with strong peaks in the *2Fo-Fc* map to assign the location of bound Cu(I) ions (Fig. 1B). Of the four monomers, one displayed anomalous electron-density peaks consistent with the presence of three Cu(I) ions with the remaining monomers consistent with the presence of four Cu(I) ions (Fig. 1B). The Cu(I) ions are coordinated by the $\text{N}^{\delta 1}$ atom of His113 and the thiolates of Cys41, Cys57, Cys104 and Cys114 (Fig. 1C). One of the Cu(I) ions, occupies the same binding

site as Cu17 in the fully Cu(I)-loaded *S/Csp3* and has an identical group III coordination sphere of Cys114/Cys57/His113.^[8] In contrast, two Cu(I) ions, although occupying similar positional locations to Cu15 and Cu18 in the fully Cu(I)-loaded *S/Csp3* structure, they are distinct in that they have an altered coordination sphere.^[8] In this respect, Cu15 (group III coordination) is not positioned close enough to the O^{δ2} atom of Asp61 to fulfil the requirements for a coordinate bond and is now assigned as group II coordination and Cu18 (group II coordination) no longer coordinates to Cys45 but instead, occupies a position enabling coordination by Cys114, but remains group II coordination (Fig. 1C). To recognise these differences compared to the fully Cu(I)-loaded structures these Cu(I) sites have been designated Cu15* and Cu18*. A fourth Cu(I) ion is present at a site, which is absent in the fully Cu(I)-loaded *S/Csp3* and we designate this as a non-cognate Cu(I) binding site with group II coordination (Fig. 1C green circle).

Group II and III dominate the coordination chemistry of the Cu(I) ions in the outer core of the four helix-bundle at low Cu(I) loading (Fig. 2A), creating a negatively charged trinuclear $[\text{Cu}_3(\mu_2\text{-S-Cys})_2(\text{S-Cys})_2(\text{N}^{\delta 1}\text{-His})]^-$ cluster and a neutral tetranuclear $[\text{Cu}_4(\mu_2\text{-S-Cys})_4(\text{N}^{\delta 1}\text{-His})]$ cluster (Fig. 2A). The latter is symmetrical in that all Cys thiolates are bridging ($\mu_2\text{-S-Cys}$) a Cu(I) ion, whereas in the trinuclear cluster this symmetry is broken as two Cys thiolates display monodentate Cu(I) coordination (Fig. 2A). The Cu-N^{δ1}(His113) bond distance is 2.1 Å in both clusters and the Cu-Sγ(Cys) bond distances range between 1.9-2.2 Å. In addition, interactions (2.5-3.1 Å) between Cu(I) ions within the $[\text{Cu}_4(\mu_2\text{-S-Cys})_4(\text{N}^{\delta 1}\text{-His})]$ cluster are observed. From the anomalous electron-density peaks, it is apparent in the trinuclear cluster that Cu15* exhibits weaker electron-density, which we attribute to a lower Cu(I) occupancy relative to the other Cu(I) coordination sites (Fig. 1B). Notably, in the $[\text{Cu}_4(\mu_2\text{-S-Cys})_4(\text{N}^{\delta 1}\text{-His})]$ cluster, the anomalous electron-density peak for Cu15* is consistent with a higher occupancy, whereas the anomalous electron-density peak for the non-cognate Cu(I) ion required to form the tetranuclear cluster has lower occupancy (Fig. 1B). This could imply that the $[\text{Cu}_4(\mu_2\text{-S-Cys})_4(\text{N}^{\delta 1}\text{-His})]$ cluster is formed in a sequential manner, whereby Cu17 and Cu18* are bound first, followed by Cu15* (trinuclear) and finally binding to the non-cognate site to create $\mu_2\text{-S-Cys57}$ and $\mu_2\text{-S-Cys104}$ coordination (Fig. 2A).

Cu(I) ions fill the inner core in a dynamic and fluxional manner

In the X-ray structure for *S/Csp3* incubated with 10 Cu(I)-equivalents, surprisingly, the anomalous electron-density maps revealed more sites occupied than Cu(I) equivalents added (Fig. 3), indicating that some of the sites are not fully occupied. In monomer A, fourteen Cu(I)

ions have been modelled into the anomalous electron-density map, with ten of these positioned in the inner core and four located in the outer core (Fig. 3). All Cu(I) ions observed in monomer A are occupying cognate sites *i.e.* found in the fully Cu(I)-loaded *S/Csp3* structure, but the anomalous electron-density peaks for Cu(I) ions 11, 12, 15*, 16 and 18* (Fig. 3), indicates reduced occupancy. Notably, no anomalous electron-density peaks are observed for sites 1, 2 and 4 in the inner core, which is also the case in the other monomers that make up the crystallographic asymmetric unit (Fig. 3). For monomer B, the anomalous electron-density map is once more consistent with the presence of fourteen Cu(I) ions. However, Cu12 and Cu16 are absent, and anomalous electron-density peaks are present for two non-cognate sites filled with Cu(I) ions, and therefore distribution of ten Cu(I) ions in the inner core and four in the outer core as found in monomer A is maintained. For monomers C and D (the latter not shown), eighteen Cu(I) ions are observed, with Cu12, Cu13 and Cu16 present, along with additional anomalous electron-density peaks located between Cu15* and 18* (green circle Fig. 3). Furthermore, Cu6, Cu8, and Cu14 have anomalous electron-density peaks consistent with lower occupancy relative to Cu(I) ions in other sites. These observations of different distributions and occupancies of Cu(I) ions within the inner and outer cores reflect a clear fluxionality of site occupancies during Cu(I) loading (Fig. 3).

An overview of the coordination chemistries of the Cu(I) ions in monomers A, B and C, together with the fully Cu(I)-loaded *S/Csp3* are illustrated in Fig. 4. In common with the 5 Cu(I)-equivalent structure, only His113 out of the three His residues at the mouth to the outer core is found to participate in coordination chemistry (Fig. 4). Furthermore, Cu15 is once more not coordinating to the O^{δ2} atom of Asp61 (Cu15*), but the O^{δ1} atom of Asp61 does maintain coordination to Cu14, albeit with a longer than average bond length of 2.8 Å compared to 2.2 Å in the fully Cu(I)-loaded structure. Notably, when Cu13 is absent (monomers A and B), Cu14 adopts a distorted tetrahedral coordination geometry (Cu14*) through coordination by Cys100, normally reserved for Cu13 (Fig. 4).

Polynuclear Cu(I)-thiolate clusters dominated by group II and III coordination are observed in the outer core for all monomers of the 10 Cu(I)-equivalent structure (Fig. 2B). In monomer B, the same neutral symmetrical tetranuclear [Cu₄(μ₂-S-Cys)₄(N^{δ1}-His)] cluster as seen in the 5 Cu(I)-equivalent structure is present (Fig. 2A and 4). However, a different tetranuclear cluster is found in monomer A, where Cys45 acts as a bridging (μ₂-S) ligand to Cu16 and Cu18*, and Cys41 as a μ₃-S ligand to Cu15*, 16 and 17 and Cys57 and Cys104 as monodentate ligands to create an asymmetric negatively charged [Cu₄(μ₃-S-Cys)(μ₂-S-

Cys)₂(S-Cys)₂(N^{δ1}-His)]⁻ cluster (Fig. 2B). Notably the Cu18* position is shifted in this cluster in respect to the other clusters and becomes three coordinate (Fig. 2B). In monomer C, the two polynuclear clusters observed in monomers A and B combine, together with a second non-cognate Cu(I) ion (green circle Fig. 4) to form a positively charged hexanuclear [Cu₆(μ₃-S-Cys)₂(μ₂-S-Cys)₃(N^{δ1}-His)]⁺ cluster (Fig. 2B). The second non-cognate Cu(I) ion in this cluster is coordinated by Cys45 and Cys57, now making the latter a μ₃-S ligand (Fig. 2B). Beyond Cu14 and into the inner core no evidence of polynuclear CuS clusters is observed and Cu(I) ions are coordinated in their respective group I or group II coordination. Therefore, these polynuclear Cu(I)-thiolate clusters are confined to the outer core and serve to illustrate the coordinative flexibility inherent within the group II and group III sites and how these can adapt to increase cluster size whilst retaining either four or five Cys thiolates as ligands (Fig. 2).

Aqueous Cu(I) can rapidly fill SICsp3 binding sites

On rapidly mixing Cu(I) with SICsp3 at sub- to super-stoichiometries with respect to the Cu(I) binding sites within SICsp3 under anaerobic conditions, optical transitions in the UV region of the absorption spectrum were observed, consistent with previously reported static titrations.^[8] The reaction time courses for the transition at 280 nm are shown in Fig. 5A. A rapid increase in absorbance is observed within the first 2 seconds followed by slower processes (Fig. 5A and B). The amplitudes of the fast processes at 280 and 310 nm (0-2 seconds of the reaction) show distinct dependences on the Cu(I) concentration (Fig. 5C), consistent with the titration of SICsp3 with Cu(I), *i.e.* below stoichiometric Cu(I) concentrations the amplitude increases linearly, indicating high affinity binding. Thereafter, (at super-stoichiometries) the amplitude plateaus, as expected for saturation of all available sites and the intersection of these two titration phases indicates a stoichiometry of Cu(I) binding of ~ 90 μM Cu(I) (Fig. 5C), consistent with 20 Cu(I) sites per monomer.^[8] Therefore, from the stopped-flow data, SICsp3 becomes fully Cu(I) loaded within 2 seconds. The rates of the loading processes seen in the time courses in Fig. 5A and B, display some Cu(I) concentration dependence, but do not conform, when analysed as sums of one or two exponentials, to second-order rate processes. This is to be expected given the complex physical chemistry of Cu(I) loading at a single site and then transferring through the monomer. For full loading to occur within 2 seconds, the individual binding sites within the monomer although having a high intrinsic affinity for Cu(I), are able to pass the Cu(I) between sites suggesting an internal ligand-exchange mechanism is operating through the monomer. Thus, our data imply that the half-life for Cu(I) dissociation

from any site within the binding tube is $\ll 2$ seconds. The slower phases seen in Fig. 5A cannot be assigned at present, but were variable in rate and amplitude, and may result from either non-specific binding or metal-induced protein-protein interactions and are not further discussed.

Cu(I) is loaded to S/Csp3 from a donor in multiple phases

Loading of aqueous Cu(I) to S/Csp3 is unlikely to occur *in vivo*. Trafficking and uptake of Cu within bacteria involves ligand-exchange type mechanisms between the metal containing donor and an acceptor,^[10] ensuring that the Cu ion remains coordinated at all times. To investigate such a process, we have used the Cu(I) nitrogen donor BCA, to monitor the kinetics of Cu(I) loading to S/Csp3. We have previously shown that S/Csp3 can remove Cu(I) from the $[\text{Cu}(\text{BCA})_2]^{3-}$ complex.^[8] On rapid mixing of S/Csp3 with $[\text{Cu}(\text{BCA})_2]^{3-}$ in the stopped-flow spectrophotometer, bleaching of the complex absorbance band centred at 562 nm was observed. The kinetics of this process are shown Figs. 6A & B. A rapid decrease in absorbance at 562 nm in Fig. 6B, illustrates Cu(I) transfer occurs within the first 2 seconds of the time monitored. Given, the high affinity of BCA for Cu(I) (implying a vanishingly small dissociation rate constant), the transfer cannot proceed with aqueous Cu(I) as an intermediate and thus must proceed via complex formation between S/Csp3 and $[\text{Cu}(\text{BCA})_2]^{3-}$. The amplitude of the absorbance change is seen to be $[\text{Cu}(\text{BCA})_2]^{3-}$ concentration dependent (Fig. 6A). Using an $\epsilon_{562 \text{ nm}} = 7,200 \text{ M}^{-1} \text{ cm}^{-1}$ for the $[\text{Cu}(\text{BCA})_2]^{3-}$ complex as determined for monitoring in the stopped-flow spectrophotometer (see Experimental Section), we indicate on Fig. 6A the expected absorbance changes for filling up to four sites in S/Csp3 (5 μM) with Cu(I). We observe that within the first 2 seconds, between 1 and 2 Cu(I) ions are delivered depending on the concentration of the $[\text{Cu}(\text{BCA})_2]^{3-}$ complex (Fig. 6B). Over a longer time-period (Fig. 6A), 80-85 % of the Cu is removed from the BCA complex, e.g. 10 μM Cu(I) of the 12.5 μM Cu(I) available. The discrepancy of the total Cu(I) available and the Cu(I)-loaded may arise either from a much slower delivery over a longer time-period that is not observed or in the experimental error of solution concentrations. Analysis of the kinetic processes showed them to comprise of at least three-exponential phases. This may be expected given that Cu(I) ions must be delivered from the $[\text{Cu}(\text{BCA})_2]^{3-}$ complex one at a time and thus involve i) complex formation between S/Csp3 and $[\text{Cu}(\text{BCA})_2]^{3-}$ (see Discussion), ii) Cu(I) transfer and iii) dissociation of the free BCA. Furthermore, sequential loading of Cu(I) implies Cu passing from site-to-site within the S/Csp3 monomer as inferred from aqueous Cu(I)-loading.

Nevertheless, we observe that the most rapid phase is most easily interpreted as transfer of a Cu(I) ion to a first coordination site in *S/Csp3*.

Structural effects of the entrance His residues on Cu(I) ion coordination

The three His residues positioned at the solvent exposed entrance to the Cys lined core in *S/Csp3* were tested for their contribution to Cu(I) binding and loading. Each His was individually replaced with Ala to create the H107A, H111A and H113A variants. Furthermore, from inspection of the X-ray structures of the partially Cu(I)-loaded *S/Csp3*, His113 was consistently found to coordinate a Cu(I) ion (Figs. 1 and 4). We therefore hypothesized that His107 and His111 could be involved in initial Cu capture and facilitate transfer to His113. Therefore, the double His-variant, H107A/H111A, was constructed. All variants were purified in the apo-state and CD spectroscopy indicated the mutations caused no significant effect to the protein fold in solution.

Addition of Cu(I) to the apo-state of the single and double His-variants under anaerobic conditions, led to the appearance of absorbance bands in the UV-spectrum that have previously been attributed in the WT protein to arise from (Cys) $S\gamma \rightarrow$ Cu(I) ligand to metal charge transfer (LMCT) bands.^[5g, 8] For all His variants the absorbance bands in the UV-region of the spectrum increase concomitantly with the Cu(I):*S/Csp3* ratio (Fig. 7A and Fig. S1). A saturation point coinciding with a stoichiometry of ~18-20 Cu(I) ions bound per monomer (Fig. 7B and Fig. S1) was observed as also noted for WT *S/Csp3* and thus, the single and double His-variants do not prevent Cu(I) loading.

To visualise the effect on the Cu(I) coordination chemistry on removing the His residues, X-ray structures of the H111A, H113A and the H107A/H111A variants after loading with 25 Cu(I)-equivalents were determined, Table 1, and the positioning of Cu(I) ions inferred through creation of anomalous electron-density maps (Fig. S2). For the H111A variant, two *S/Csp3* monomers were identified in the crystallographic asymmetric, whereas only one *S/Csp3* monomer was found in the H113A and H107A/H111A variant structures. Suitable diffraction quality crystals for the H107A variant were not obtained. From the anomalous electron-density maps (Fig. S2), it is apparent that for all variants the inner core, housing Cu(I) ions 1-14 retains identical coordination chemistry to the WT *S/Csp3*, however, some variation is observed in the outer core (Fig. S2). For all variants, a non-cognate site is filled by a Cu(I) ion and is located adjacent to Cu15 and coordinated by the $O^{\delta 1}$ of Asp61 and only one thiolate from Cys 57, creating a group III site (Fig. 8 green circle). In the H111A and H107A/H111A structures both

Cu19 and 20 are notable by their absence, implying that H111 and H107 are important for initial Cu(I) loading. Removal of His113 results in the absence of Cu17 (Fig. 8), but would appear to release steric constraints enabling for the side chain of His111 to adopt an alternative conformation to that observed in the WT *S/Csp3* structure resulting in coordination to Cu20 (Fig. 8). It is further noted that in one of the H111A monomers a second non-cognate Cu(I) ion is present that shares coordination of the N^{δ1} atom of His113 with Cu17, and leads to μ₃-S-Cys41 coordination. This brings the total number of Cu(I) ions bound to twenty in one H111A monomer (nineteen in the other), eighteen cognate sites and two non-cognate sites, and further underscores the adaptability and flexibility of Cu(I) coordination sites within the outer core of these proteins.

His107 is important for initial Cu(I) entry

To probe further the mechanism of the initial Cu(I)-loading to *S/Csp3*, stopped-flow kinetics of the His-variants with the [Cu(BCA)₂]³⁻ complex as the donor was carried out. Figure 9 compares the loading of Cu(I) to the WT *S/Csp3* and the His variants with the expected optical density change for filling one site with Cu(I) indicated. Over the first 2 seconds, rapid transfer is observed (Fig. 9A) and it is apparent that the H111A and H113A variants are essentially indistinguishable from the WT *S/Csp3*, whereas the H107A and the H107A/H111A double variant clearly show that entry of Cu(I) is perturbed (Fig. 9A). This implies that H107A has a major role in initial Cu(I) transfer. Over a longer time-period, during which ~ 80% of the available Cu(I) can be delivered to the WT *S/Csp3*, further effects of the His-variants may be discerned (Fig. 9B). The H107A variant identified as important in initial entry, slows subsequent loading (Fig. 9B), whereas the H111A variant, while not effecting the initial entry does further slow Cu(I) entry (Fig. 9B). Of note, the double variant which is similar to H107A in affecting the initial entry, has a significant effect on subsequent loading (Fig. 9B). Examination of the structure in Fig. 4D and these data, indicate H107 and H111 are important ligands to the first two Cu(I) sites (19 and 20). The H113A variant affects neither the initial entry nor subsequent loading of up to at least four Cu(I) ions per monomer, suggesting that the removal of this coordinating His does not impair binding to the site or impair transfer from the initial entry sites to other available sites.

DISCUSSION

The capacity to bind multiple Cu(I) ions through predominately thiolate coordination chemistries to protect bacteria against potential toxicity is an inherent feature of the recently discovered Csp3 members.^[6c] Understanding the kinetic and thermodynamic intricacies associated with Cu(I) loading to these proteins is particularly challenging considering the number of potential binding sites (cognate and non-cognate) that Cu(I) thiolate chemistry can impose. Below we summarise our results and then attempt to rationalise our findings by constructing a model of Cu(I) binding in terms of the relative energy of binding to the distinct Cu(I) sites in *Sl*Csp3.

An initial binding complex is not directly observed when using aqueous Cu(I) to load *Sl*Csp3 as implied by the lack of second-order binding kinetics (*i.e.* no linear dependence of k_{obs} on Cu(I) concentration). Such a complex must be present in the initial binding step and is a situation reminiscent of Cu(I) loading to other proteins which we have studied, whereby rapid metal ion binding may be inferred but not directly observed.^[13] It seems reasonable to suggest that this complex involves initial His binding to Cu(I), which is expected to be optically silent as proposed earlier.^[13b]

At low Cu(I) to protein ratios, Cu sites 15*, 17 and 18* are loaded with variable occupancy and a trinuclear $[\text{Cu}_3(\mu_2\text{-S-Cys})_2(\text{S-Cys})_2(\text{N}^{\delta 1}\text{-His})]^-$ and a tetranuclear $[\text{Cu}_4(\mu_2\text{-S-Cys})_4(\text{N}^{\delta 1}\text{-His})]$ cluster, with the fourth Cu(I) occupying a non-cognate site is visualised in the outer core (Fig. 2A). Sites 19 and 20 remain empty but they must participate in Cu(I)-loading. It is notable from the structural studies of partially loaded *Sl*Csp3 that Cu(I) occupancy at sites 19 and 20 is only observed in the fully Cu(I)-loaded structure, and in the case of the His variants, sites 19 and 20 are only occupied when His107 and His111 are together present (Fig. 8). Thus, sites 19 and 20 may be considered as transient loading sites or entrance sites to the outer core. Dennison and co-workers using X-ray crystallography also visualised an initial $[\text{Cu}_4(\mu_2\text{-S-Cys})_4]$ cluster forming, but in the inner core of *Mt*Csp3 under low Cu(I) loading conditions.^[12] This contrasts to our observation, in *Sl*Csp3, where we visualise the formation of a $[\text{Cu}_4(\mu_2\text{-S-Cys})_4]$ cluster in the outer core.

At low Cu(I) loadings (5 Cu(I)-equivalents), sites 1-14 remain empty, implying an energetic barrier to the distribution of Cu(I) beyond the initial tetranuclear cluster formed in the outer core must exist. Thus, the $[\text{Cu}_4(\mu_2\text{-S-Cys})_4]$ cluster must be thermodynamically more favoured than occupancy of the sites available in the inner core, at least under low Cu(I) to protein ratios. On addition of 10 Cu(I)-equivalents, sites within the inner core become occupied, with it noted that variability in site occupancy between different chains of the

homotetramer exist, implying flexibility and fluxionality of Cu(I) in the protein during loading. Furthermore, sites 1, 2 and 4 display similar traits to sites 19 and 20 in that occupancy is only observed when *S/Csp3* becomes fully Cu(I) loaded (Fig. 3 and 4).

A model to describe Cu(I) binding in terms of the relative energy of binding to the distinct Cu(I) sites is depicted in Fig. 10 and illustrates the relative stability of the complexes of Cu(I) in the sites described. When Cu(I) transfer is from the $[\text{Cu}(\text{BCA})_2]^{3-}$ complex, this must occur via a ligand-substitution mechanism to account for the relatively fast transfer (Fig. 6). As the tetrahedral $[\text{Cu}(\text{BCA})_2]^{3-}$ complex is coordinatively saturated we suggest that on mixing with *S/Csp3* a heteroleptic complex forms, consisting of $[\text{Cu}(\text{BCA})]^-$ and a nitrogen from a His residue with the net loss of a BCA ligand (Fig. 10). We identify this His residue as His107 from the initial phase of the kinetic time course (Fig. 9A). Following this step, an energetically favourable transfer to sites 19 and 20 will occur, which structurally would involve both His and Cys coordination (group III). Sites 19 and 20 are transiently filled and Cu(I) is transferred to sites 15*, 17 and 18* causing release of His107 from coordination and enabling for further Cu(I) capture from the donor (His-ligand cycle, Fig. 10). The trinuclear cluster that we visualise in one of the monomers at 5 Cu(I)-equivalents may therefore be considered as a higher energy cluster on the way to forming the more thermodynamically stable tetranuclear cluster (Figs. 2A and 10).

Figure 9B shows that over a longer reaction time course, both His107 and His111 slow Cu(I) loading beyond sites 19 and 20 and their effects are additive. We account for these results by reference to the crystal structure that indicates both His residues are involved in binding and stabilising Cu(I) in sites 19 and 20. The removal of these residues may lead to a decrease in the Cu(I) loading to these sites and hence to a slowing of loading to the interior of the protein as this must occur from Cu(I) populated at sites 19 and 20. Furthermore, as we have identified His107 as important for a ligand-exchange mechanism of moving Cu(I) from BCA, we may expect this residue to have a marked effect, because in order for up to four Cu(I) ions to load as illustrated in Fig. 9B, the $[\text{Cu}(\text{BCA})]^-$ -His-*S/Csp3* complex must form, transfer Cu(I) and dissociate after each Cu(I) is donated. Thus, for four Cu(I) ions loaded, the His-ligand cycle must occur four times and as each loading requires His107 for efficient transfer its absence would have a significant effect on the loading and could account for the observed kinetics (Fig. 9B).

At low Cu(I) stoichiometry, Cu(I) transfer beyond site 15* is not observed. Thus, the formation of the $[\text{Cu}_4(\mu_2\text{-S-Cys})_4(\text{N}^{\delta 1}\text{-His})]$ cluster creates an unfavourable barrier to loading

into the inner core (Fig. 10). A reason for this may be that to move Cu(I) into the inner core via the binding sites 15 and 14, interaction with Asp61 must occur (Asp sites Fig. 10). A hard ligand/soft metal interaction is less favoured and of lower affinity than the Cu(I) thiolate coordination dominating the tetranuclear cluster. However, as more Cu(I) is loaded into the outer core this barrier can be overcome, leading to transfer into the inner core becoming favourable. This accounts for our observation that at 10 Cu(I)-equivalents Cu(I) ions are present in both cores (Fig. 3).

The model depicted in Fig. 10, also gives insight into how *S/Csp3* achieves very high affinity for Cu(I) while retaining rapid kinetic transfer. A mathematical analysis of a multi-site protein (up to 20 sites) is complex and requires solutions of at least quartic equations. However, without resorting to such complexity it is possible to see that the dissociation constant (K_d) for *S/Csp3*, defined as the free Cu(I) concentration in solution at equilibrium with the protein at half saturation, arises from the K_d of the initial Cu(I) capture site, which is likely to be of the order 10^{-5} M (typical for Cu(I) His interaction^[13a, 13b]) divided by a function of the multiple of the equilibrium constants for transfer from the capture complex to sites 19 and 20, sites 15*, 17 and 18* and so on. Overall this multiple will be large and positive, resulting in the extremely small K_d value (10^{-17} M) measured for *S/Csp3*.^[8]

CONCLUSIONS

In conclusion, this study offers the first insight into the kinetics of Cu(I) loading to a non-methanotrophic Csp3 member and in particular highlights that the His residues at the hydrophilic mouth of the outer core are the entrance sites of Cu(I) loading. We illustrate that rapid and efficient kinetic transfer occurs from an organic Cu(I) nitrogen donor to *S/Csp3*. *In vivo* potential Cu(I) donors to *S/Csp3* could involve Cu chaperone proteins that utilise digonal bis-cysteinate coordination,^[9, 11a, 14] and thus the kinetics of Cu(I) transfer to a Csp3 may differ from a thiol Cu(I) donor compared to a nitrogen donor. However, chalkophores, natural products produced by bacteria that chelate and transport copper,^[7, 15] predominately utilise nitrogen as a Cu(I) donor, as is the case here with the $[\text{Cu}(\text{BCA})_2]^{3-}$ complex. Until recently chalkophores have been associated with methanotrophic bacteria.^[15a] Interestingly, diisonitrile derivatives with nitrogen and/or oxygen as Cu(I) donor, with 1:2 (Cu(I):ligand) stoichiometry, have been discovered in *Streptomyces thioluteus* and identified to play a role in Cu uptake mechanisms.^[16] This poses the question of whether similar compounds serve as donors to Csp3s, as opposed to thiol donors such as CopZ Cu chaperones. Thus, our kinetic studies of Cu(I) transfer to *S/Csp3* utilizing a nitrogen Cu(I) donor in the guise of the $[\text{Cu}(\text{BCA})_2]^{3-}$

complex and the discovery of role for a His residue in facilitating the Cu(I) transfer bear significance on potential biological events. Finally, structural studies further indicate that the driving force to sequester Cu(I) and prevent toxicity by Csp3 members is through the initial formation of tetranuclear Cu(I)-thiolate clusters.^[6c, 12] Contrary to cluster formation in the inner core as revealed in *MtCsp3*, a tetranuclear cluster forms in the outer core of *SlCsp3* and its presence affects the loading of the inner core at low Cu(I) loading.

EXPERIMENTAL SECTION

Site-directed mutagenesis, over-expression and purification of SlCsp3

Mutagenic primers to create the desired nucleotide changes to generate the His variants in *SlCsp3* were designed and synthesised (Sigma-Aldrich) and the Quikchange mutagenesis strategy (Stratagene) employed (see Supporting Information). Mutant clones were corroborated for the presence of the desired mutation by DNA sequencing (Source Bioscience). Recombinant production of wild-type (WT) *SlCsp3* and the His variants in *Escherichia coli* BL21(DE3) cells and purification was carried out as previously described.^[8] Far UV-circular dichroism spectroscopy using an Applied Photophysics Chirascan CD spectrometer (Leatherhead, UK) was used to assess whether the proteins were folded. All proteins were stored at -20 °C until required.

Preparation of proteins, Cu(I) solutions and complexes

Apo-*SlCsp3* proteins were exchanged into 10 mM MOPS pH 7.5, 150 mM NaCl. For Cu(I)-titrations and stopped-flow kinetics samples were prepared together with CuCl solutions in an anaerobic chamber (DW Scientific [O₂] < 2 ppm). Solid CuCl (Sigma-Aldrich) was dissolved in 100 mM HCl and 1 M NaCl and diluted with 10 mM MOPS pH 7.5, 150 mM NaCl. The Cu(I) concentration was determined spectrophotometrically using a Cary 60 UV-visible spectrophotometer (Varian) thermostatted at 20 °C through step-wise addition of the stock CuCl solution into a known concentration of the Cu(I) specific bidentate chelator bicinchoninic acid (BCA; Sigma-Aldrich). Formation of the [Cu(BCA)₂]³⁻ complex was monitored using absorption spectroscopy by following the increase in absorbance at 562 nm on addition of Cu(I) and the concentration determined using an extinction coefficient (ϵ) of 7,900 M⁻¹ cm⁻¹.^[17]

X-ray crystallography

Under anaerobic conditions WT *S/Csp3* (0.2 mM) was incubated with 5, 10 and 25 molar equivalents of CuCl, and to the His variants (0.15 to 0.39 mM) 25 molar equivalents of CuCl were added. Unbound Cu(I) was removed by passing samples through a PD-10 column (Generon) and the protein was removed from the anaerobic chamber and concentrated to ~ 10-15 mg/ml using centrifugal concentration (Vivaspin 20). Crystallisation of the Cu(I)-loaded samples was screened around 1.4 to 1.6 ammonium sulfate, 0.1 M MES pH 6.0 by mixing equal (1 μ l) volumes of protein and reservoir solution. Crystals were transferred to a cryoprotectant solution consisting of precipitants and 40 % w/v sucrose, and flash cooled by plunging into liquid nitrogen. WT Cu-loaded *S/Csp3* crystals were measured at the Swiss Light Source on beamline XS10A using an X-ray wavelength of 1.33 Å (where only the Cu K-edge contributes to the anomalous scattering) and a Pilatus 6M-F detector. Crystals of the His variants were measured at the Diamond Light Source on beamline I04 using an X-ray wavelength of 0.979 Å and a Pilatus 6M-F detector. Data from SLS were indexed using XDS^[18] and scaled and merged using Aimless^[19] in the CCP4 suite with the CCP4i2 interface.^[20] Data from DLS were autoprocessed in DIALS using Xia2^[21] and Aimless.^[19] Structures were solved by molecular replacement in MOLREP^[22] using the apo-*S/Csp3* structure (PDB ID 6EI0) as the search model.^[8] Cycles of model building in Coot^[23] and refinement in Refmac5^[24] were carried out and riding hydrogen atoms were added when refinement of the protein atoms had converged. For all data sets anomalous difference maps for validation of Cu atom positions was generated using PHASER^[25] in the CCP4i2 interface. Structures were validated using the Molprobtity server^[26] the JCSG Quality Control Server and tools within Coot.^[23] Coordinates and structure factors were deposited in the RCSB Protein Data Bank. A summary of data, refinement statistics and the quality indicators for the structures are given in Table 1.

Stopped-flow absorption spectroscopy

An Applied Photophysics (Leatherhead, UK) stopped-flow spectrophotometer operating in absorbance mode using either a photomultiplier capture system or diode array and thermostatted to 20 °C was employed to monitor the kinetics of Cu(I)-loading to *S/Csp3* and the His variants. Anaerobic buffers were prepared by repeated exposure to vacuum followed by equilibration with oxygen free argon. Buffers were taken into glass syringes equipped with coupling tubes allowing dilution of the anaerobic Cu(I) solutions without exposure to oxygen. Protein solutions were prepared by similar cycles of gentle degassing and equilibration with oxygen free argon. The stopped-flow apparatus was washed through with anaerobic buffer

prior to introduction of the reactants (protein and Cu(I)) under study. This procedure permits reactions to be studied at oxygen concentrations of 2 μM or below. The appropriate extinction coefficient (accounting for the slit-width used in the stopped-flow experiments and wavelength discrimination in the diode array) for bleaching the $[\text{Cu}(\text{BCA})_2]^{3-}$ complex on Cu(I) removal was determined by mixing a known concentration the $[\text{Cu}(\text{BCA})_2]^{3-}$ complex (200 μM) with an excess of protein and monitoring full bleaching of the absorption band at 562 nm using the diode array. The value of this apparent $\epsilon_{562\text{nm}}$ was found to be 7,200 $\text{M}^{-1} \text{cm}^{-1}$. This value constitutes ~ 90 % of the literature value.^[17]

CONFLICTS OF INTEREST

There are no conflicts to declare

ACKNOWLEDGEMENTS

MLS acknowledges the Eastern Arc consortium for a SynBio PhD studentship. The authors would like to thank Diamond Light Source for beamtime (BAG proposal mx13467), and the Swiss Light Source (proposal 20160704). We thank Dr Florian Dworkowski for assistance with data collection at the Swiss Light Source.

REFERENCES

- [1] R. A. Festa, D. J. Thiele, *Curr. Biol.* **2011**, *21*, R877-883.
- [2] ^aA. Sykes, *Adv Inorg Chem* **1991**, *36*, 377-408; ^bP. Tavares, A. S. Pereira, J. J. Moura, I. Moura, *J Inorg Biochem* **2006**, *100*, 2087-2100; ^cE. I. Solomon, D. E. Heppner, E. M. Johnston, J. W. Ginsbach, J. Cirera, M. Qayyum, M. T. Kieber-Emmons, C. H. Kjaergaard, R. G. Hadt, L. Tian, *Chem Rev* **2014**, *114*, 3659-3853.
- [3] ^aL. Macomber, C. Rensing, J. A. Imlay, *J Bacteriol* **2007**, *189*, 1616-1626; ^bL. Macomber, J. A. Imlay, *Proc Natl Acad Sci U S A* **2009**, *106*, 8344-8349; ^cS. Chillappagari, A. Seubert, H. Trip, O. P. Kuipers, M. A. Marahiel, M. Miethke, *J Bacteriol* **2010**, *192*, 2512-2524; ^dA. Azzouzi, A. S. Steunou, A. Durand, B. Khalfoui-Hassani, M. L. Bourbon, C. Astier, D. W. Bollivar, S. Ouchane, *Mol Microbiol* **2013**, *88*, 339-351; ^eK. Y. Djoko, A. G. McEwan, *ACS Chem Biol* **2013**, *8*, 2217-2223.
- [4] ^aB. E. Kim, T. Nevitt, D. J. Thiele, *Nat Chem Biol* **2008**, *4*, 176-185; ^bK. J. Waldron, J. C. Rutherford, D. Ford, N. J. Robinson, *Nature* **2009**, *460*, 823-830; ^cN. J. Robinson, D. R. Winge, *Annu Rev Biochem* **2010**, *79*, 537-562; ^dC. Rademacher, B. Masepohl, *Microbiology* **2012**, *158*, 2451-2464; ^eJ. M. Arguello, D. Raimunda, T. Padilla-Benavides, *Front Cell Infect Microbiol* **2013**, *3*, 73.
- [5] ^aT. D. Rae, P. J. Schmidt, R. A. Pufahl, V. C. Culotta, T. V. O'Halloran, *Science* **1999**, *284*, 805-808; ^bA. Changela, K. Chen, Y. Xue, J. Holschen, C. E. Outten, T. V. O'Halloran, A. Mondragon, *Science* **2003**, *301*, 1383-1387; ^cL. A. Finney, T. V. O'Halloran, *Science* **2003**, *300*, 931-936; ^dA. V. Davis, T. V. O'Halloran, *Nat Chem Biol* **2008**, *4*, 148-151; ^eB. Gold, H. Deng, R. Bryk, D. Vargas, D. Eliezer, J. Roberts,

- X. Jiang, C. Nathan, *Nat Chem Biol* **2008**, *4*, 609-616; ^fK. Helbig, C. Bleuel, G. J. Krauss, D. H. Nies, *J Bacteriol* **2008**, *190*, 5431-5438; ^gN. Vita, S. Platsaki, A. Basle, S. J. Allen, N. G. Paterson, A. T. Crombie, J. C. Murrell, K. J. Waldron, C. Dennison, *Nature* **2015**, *525*, 140-143; ^hP. Chandrangsu, V. V. Loi, H. Antelmann, J. D. Helmann, *Antioxid Redox Signal* **2018**, *28*, 445-462.
- [6] ^aN. Vita, G. Landolfi, A. Basle, S. Platsaki, J. Lee, K. J. Waldron, C. Dennison, *Sci Rep* **2016**, *6*, 39065; ^bC. Dennison, S. David, J. Lee, *J Biol Chem* **2018**, *293*, 4616-4627; ^cC. Dennison, *Chemistry* **2019**, *25*, 74-86.
- [7] A. A. DiSpirito, J. D. Semrau, J. C. Murrell, W. H. Gallagher, C. Dennison, S. Vuilleumier, *Microbiol Mol Biol Rev* **2016**, *80*, 387-409.
- [8] M. L. Straw, A. K. Chaplin, M. A. Hough, J. Paps, V. N. Bavro, M. T. Wilson, E. Vijgenboom, J. A. R. Worrall, *Metallomics* **2018**, *10*, 180-193.
- [9] D. L. Huffman, T. V. O'Halloran, *J Biol Chem* **2000**, *275*, 18611-18614.
- [10] D. T. Richens, *Chem Rev* **2005**, *105*, 1961-2002.
- [11] ^aA. K. Wernimont, D. L. Huffman, A. L. Lamb, T. V. O'Halloran, A. C. Rosenzweig, *Nat Struct Biol* **2000**, *7*, 766-771; ^bL. Banci, I. Bertini, F. Cantini, I. C. Felli, L. Gonnelli, N. Hadjiliadis, R. Pierattelli, A. Rosato, P. Voulgaris, *Nat Chem Biol* **2006**, *2*, 367-368; ^cA. K. Boal, A. C. Rosenzweig, *Chem Rev* **2009**, *109*, 4760-4779; ^dA. Badarau, C. Dennison, *J Am Chem Soc* **2011**, *133*, 2983-2988.
- [12] A. Basle, S. Platsaki, C. Dennison, *Angew Chem Int Ed* **2017**, *56*, 8697-8700.
- [13] ^aK. L. Blundell, M. T. Wilson, E. Vijgenboom, J. A. Worrall, *Dalton Trans* **2013**, *42*, 10608-10616; ^bT. V. Porto, M. T. Wilson, J. A. Worrall, *Dalton Trans* **2015**, *44*, 20176-20185; ^cA. K. Chaplin, D. A. Svistunenko, M. A. Hough, M. T. Wilson, E. Vijgenboom, J. A. Worrall, *Biochem J* **2017**, *474*, 809-825.
- [14] ^aF. Arnesano, L. Banci, I. Bertini, D. L. Huffman, T. V. O'Halloran, *Biochemistry* **2001**, *40*, 1528-1539; ^bD. L. Huffman, T. V. O'Halloran, *Annu Rev Biochem* **2001**, *70*, 677-701.
- [15] ^aH. J. Kim, D. W. Graham, A. A. DiSpirito, M. A. Alterman, N. Galeva, C. K. Larive, D. Asunskis, P. M. Sherwood, *Science* **2004**, *305*, 1612-1615; ^bR. Balasubramanian, A. C. Rosenzweig, *Curr Opin Chem Biol* **2008**, *12*, 245-249; ^cS. Yoon, S. M. Kraemer, A. A. DiSpirito, J. D. Semrau, *Environ Microbiol Rep* **2010**, *2*, 295-303.
- [16] L. Wang, M. Zhu, Q. Zhang, X. Zhang, P. Yang, Z. Liu, Y. Deng, Y. Zhu, X. Huang, L. Han, S. Li, J. He, *ACS Chem Biol* **2017**, *12*, 3067-3075.
- [17] Z. Xiao, P. S. Donnelly, M. Zimmermann, A. G. Wedd, *Inorg Chem* **2008**, *47*, 4338-4347.
- [18] W. Kabsch, *Acta Crystallogr D* **2010**, *66*, 125-132.
- [19] P. R. Evans, G. N. Murshudov, *Acta Crystallogr D*, **2013**, *69*, 1204-1214.
- [20] L. Potterton, J. Agirre, C. Ballard, K. Cowtan, E. Dodson, P. R. Evans, H. T. Jenkins, R. Keegan, E. Krissinel, K. Stevenson, A. Lebedev, S. J. McNicholas, R. A. Nicholls, M. Noble, N. S. Pannu, C. Roth, G. Sheldrick, P. Skubak, J. Turkenburg, V. Uski, F. von Delft, D. Waterman, K. Wilson, M. Winn, M. Wojdyr, *Acta Crystallogr D*, **2018**, *74*, 68-84.
- [21] G. Winter, *J Appl Crystallogr* **2010**, *43*, 186-190.
- [22] A. Vagin, A. Teplyakov, *J Appl Crystallogr* **1997**, *30*, 1022-1025.
- [23] P. Emsley, K. Cowtan, *Acta Crystallogr D*, **2004**, *60*, 2126-2132.
- [24] G. N. Murshudov, A. A. Vagin, E. J. Dodson, *Acta crystallogr*, **1997**, *53*, 240-255.
- [25] A. J. McCoy, R. W. Grosse-Kunstleve, P. D. Adams, M. D. Winn, L. C. Storoni, R. J. Read, *J Appl Crystallogr* **2007**, *40*, 658-674.

- [26] I. W. Davis, A. Leaver-Fay, V. B. Chen, J. N. Block, G. J. Kapral, X. Wang, L. W. Murray, W. B. Arendall, 3rd, J. Snoeyink, J. S. Richardson, D. C. Richardson, *Nucleic Acids Res* **2007**, *35*, W375-383.

Table 1: Crystallographic data processing and refinement statistics for the various forms of *SlCsp3* used in this work. Values in parenthesis refer to the outermost resolution shell.

Structure	Ccsp-5Cu	Ccsp-10Cu	H111A	H113A	H107A/H11A
Space group	P6 ₁ 22	P6 ₁ 22	P2 ₁ 2 ₁ 2	I222	I222
Unit cell (Å)	93.1, 93.1, 212.3	93.4, 93.4, 216.0	65.3, 62.2, 65.2	62.2, 65.1, 65.3	62.2, 64.0, 65.7
Resolution (Å)	75.4-1.50	75.8-1.90	65.3-1.20	32.7-1.30	44.6-1.20
Unique reflections	85587 (3492)	44544 (2831)	86182 (3562)	33353 (1526)	42048 (1551)
Mn (I/SD)	19.5 (1.3)	12.8 (1.2)	17.6 (1.2)	23.7 (1.4)	18.6 (1.0)
CC _{1/2}	0.99 (0.45)	0.99 (0.46)	0.99 (0.61)	0.99 (0.59)	0.99 (0.50)
Completeness (%)	98.0 (82.5)	99.7 (100)	98.1 (81.6)	96.7 (89.2)	96.9 (73.1)
Redundancy	8.0 (8.7)	9.1 (9.2)	6.3 (3.3)	7.3 (7.3)	7.1 (4.1)
R _{cryst}	0.195	0.218	0.182	0.161	0.168
R _{free}	0.214	0.255	0.194	0.187	0.192
RMS dev. bond lengths (Å)	0.013	0.015	0.0064	0.0052	0.0079
RMS dev. bond angles (°)	1.47	1.64	1.40	1.33	1.48
Ramachandran favoured (%)	99.8	98.2	100.0	96.7	100.0
PDB accession code	6Q58	6Q6B	6QYB	6QVH	6R01

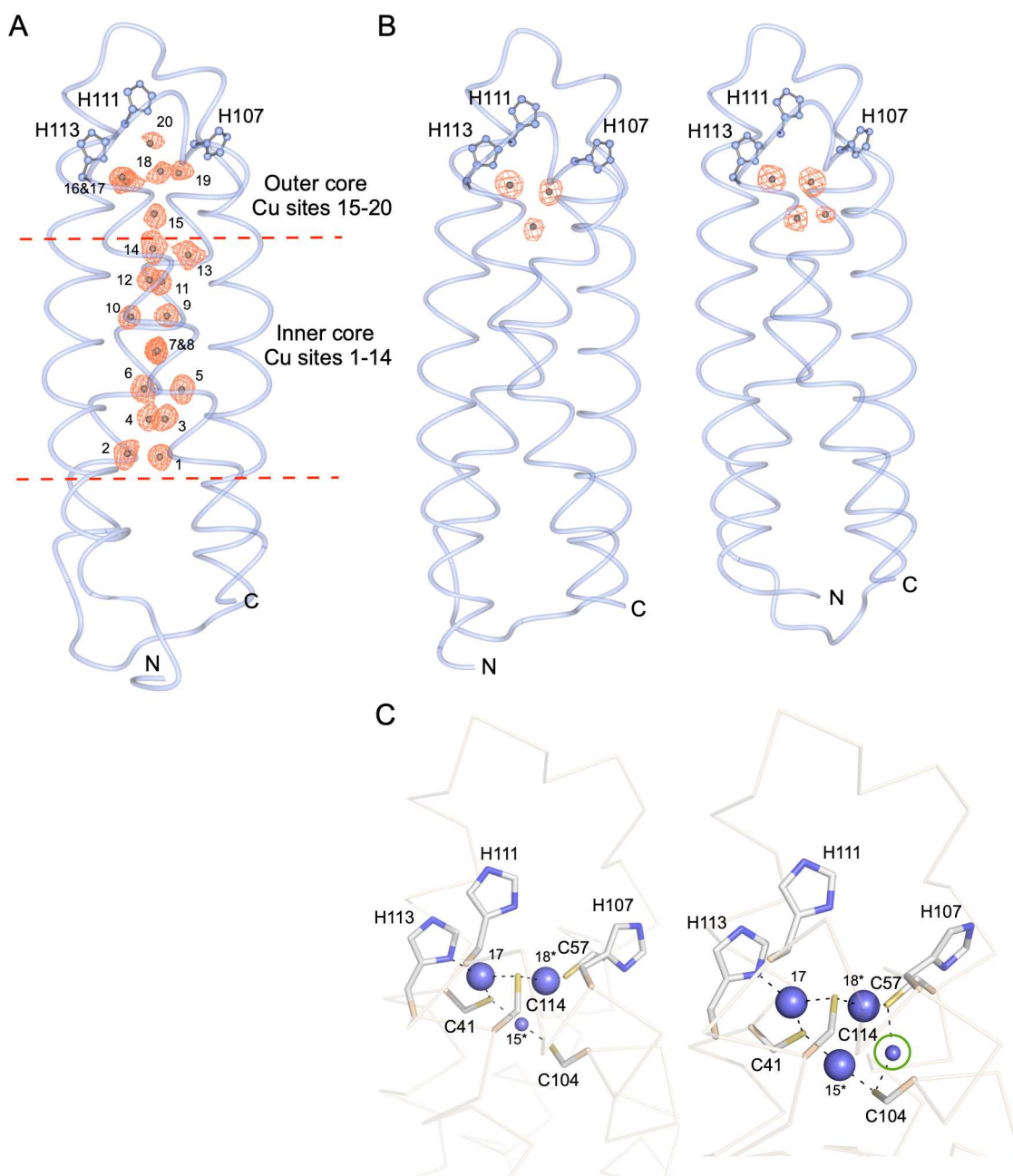


Figure 1: Location of Cu(I) sites in fully and partially Cu(I)-loaded *S/Csp3* determined by X-ray crystallography. The location of bound Cu(I) ions are inferred by the anomalous electron-density peaks shown in orange mesh and contoured at 5σ . A) Fully Cu(I)-loaded structure with the location and the number of Cu(I) ions found in the inner and outer cores indicated by dashed red lines (PDB 6EK9).^[8] B & C) 5 Cu(I)-equivalent structures. B) Two monomers showing three and four Cu(I) bounds, respectively. C) Coordination chemistries found in the outer core of the two promoters in (B), with Cu(I) ions represented in blue spheres and coordinate bonds as dashed lines. The smaller spheres indicate partial occupancy based on the anomalous electron-density peaks, and the green circle indicates a non-cognate site with a Cu(I) ion bound.

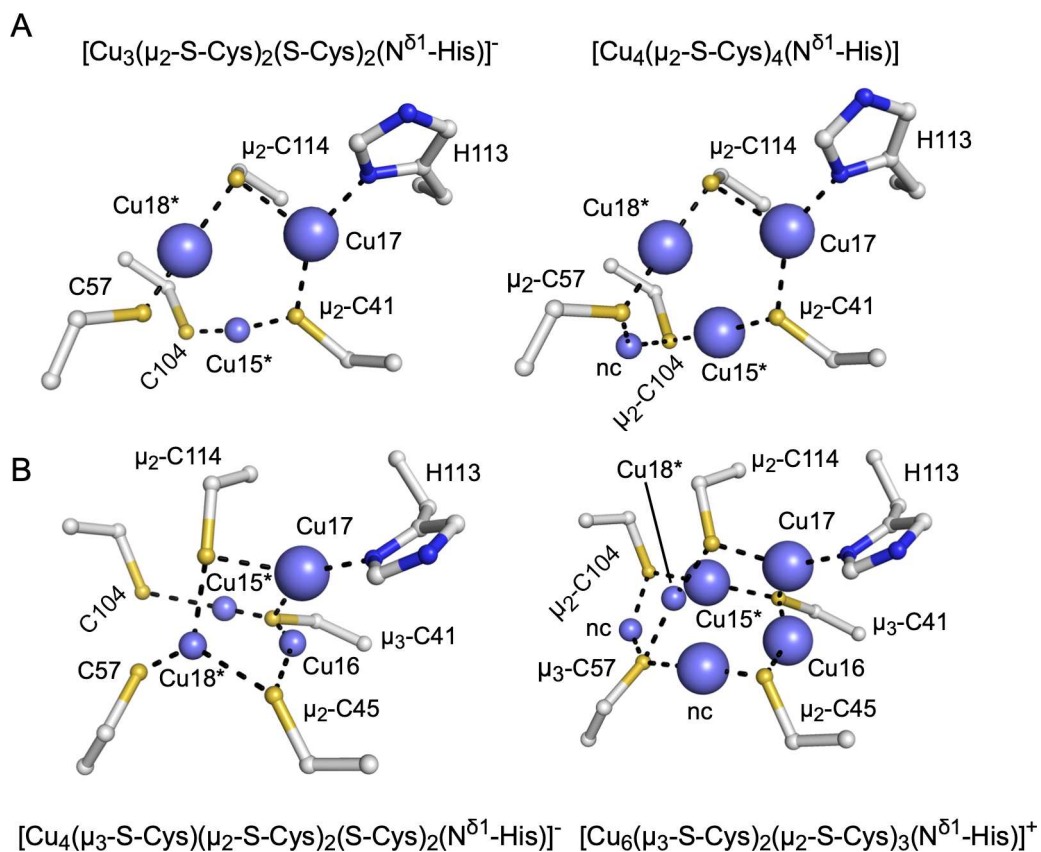


Figure 2: Polynuclear Cu(I) clusters present in the outer core of *S/Csp3*. The clusters present in the 5 Cu(I)-equivalent structure (A) and the 10 Cu(I)-equivalent structure (B). The Cu(I) ions (blue spheres) bound at non-cognate sites are labeled, nc, and the smaller blue spheres indicate a lower occupancy as determined from the anomalous electron-density peaks.

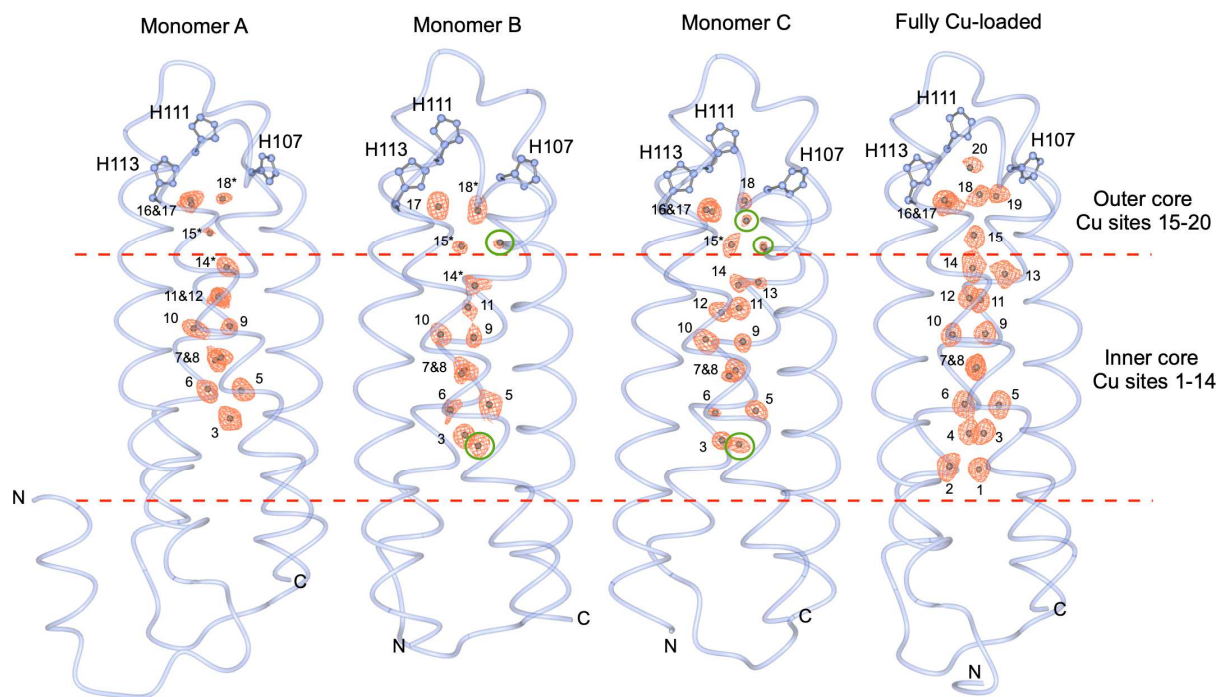


Figure 3: X-ray structures of *S/Csp3* with 10 Cu(I)-equivalents added. Monomers A, B and C are represented with the fully Cu(I)-loaded structure (PDB 6EK9)^[8] shown for comparison. Anomalous electron-density for the Cu(I) ions is depicted in orange mesh and contoured at 5σ . Green circles indicate the location of non-cognate sites containing a Cu(I) ion. In monomer A, electron-density is present in the asymmetric unit that enables for additional residues to be modeled at the N-termini, which now starts at residue 7, as opposed to residue 15 in the other monomers in the crystallographic asymmetric unit.

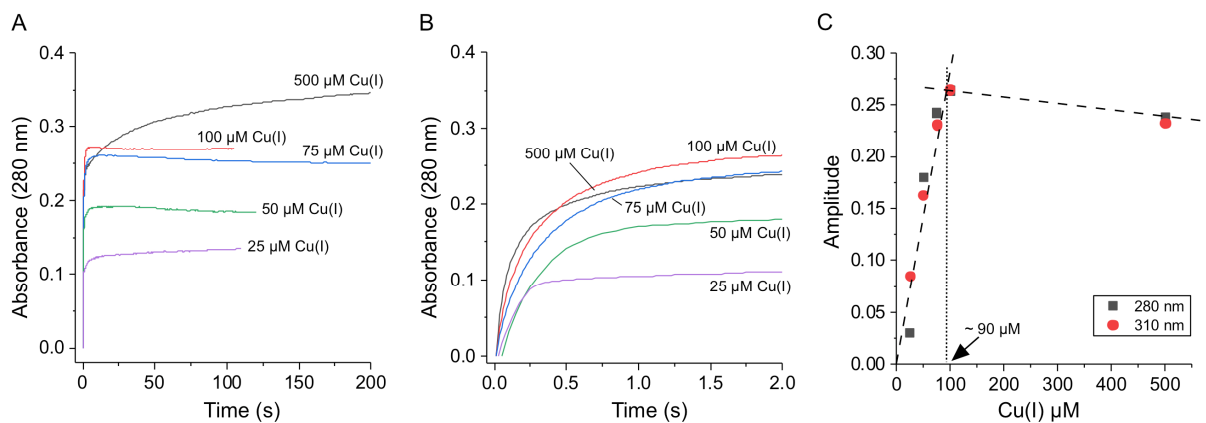


Figure 5: Kinetics of aqueous Cu(I) loading to *SICsp3*. A) and B) Stopped-flow reaction time-courses monitored at 280 nm on mixing increasing concentrations of CuCl under anaerobic conditions. A fast phase between 0-2 seconds is observed (B), followed by slower phases over timescales up to 200 s (A). C) The amplitudes of the fast phase (between 0-2seconds) observed at 280 nm and 310 nm plotted against increasing concentrations of Cu(I). The intersection of the two dashed lines is indicated revealing a saturating Cu(I) concentration of ~ 90 μM . Experiments were performed at 20 °C in 10 mM MOPS pH 7.5, 150 mM NaCl with 4.5 μM of *SICsp3* after mixing. Solutions of Cu(I) at known concentration were obtained from dilution of a 1mM stock CuCl solution under anaerobic conditions.

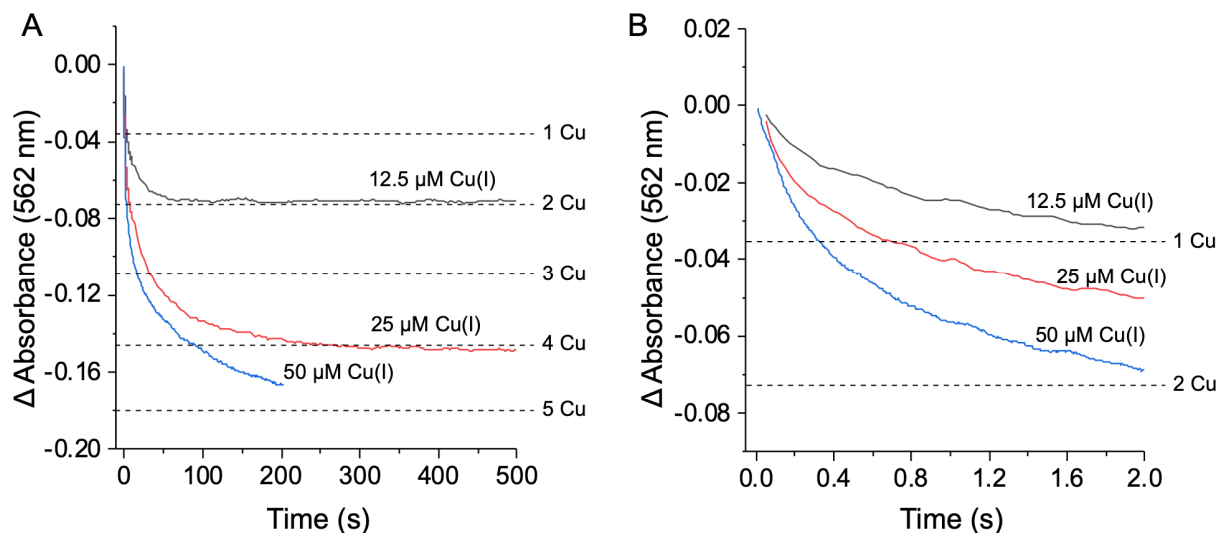


Figure 6: Kinetics of Cu(I) loading to S/Csp3 from the [Cu(BCA)₂]³⁻ complex. A) and B) stopped-flow reaction time-courses monitored at 562 nm on mixing S/Csp3 (5 μ M) with increasing concentrations of Cu(I) chelated in the [Cu(BCA)₂]³⁻ complex revealing an initial fast phase (B) followed by slower phases (A). Dashed lines indicate the expected absorbance changes for removal of Cu(I) equivalents from the [Cu(BCA)₂]³⁻. Up to 50 μ M [Cu(BCA)₂]³⁻ complex the kinetics could be monitored satisfactorily for the first 200 seconds, thereafter, at longer times and at higher [Cu(BCA)₂]³⁻ concentrations, interactions between [Cu(BCA)₂]³⁻ complexes themselves perturbed the spectra and made it impossible to analyse confidently the data in terms of Cu(I) transfer to S/Csp3. Experiments were performed at 20 °C in 10 mM MOPS pH 7.5, 150 mM NaCl.

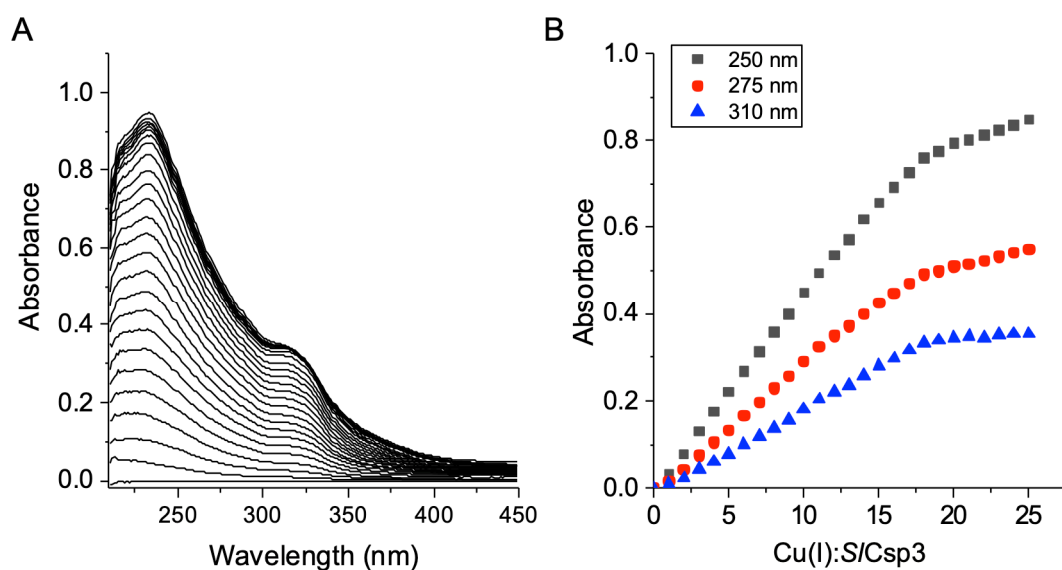


Figure 7: Cu(I) titration to the *S/Csp3* H107A/H111A variant. A) UV-vis difference spectrum upon titration of a stock solution of CuCl to 5.6 μ M of the protein revealing the appearance of (Cys) S_{γ} \rightarrow Cu(I) LMCT bands. B) Plots of absorbance versus the Cu(I):*S/Csp3* concentration ratio at selected wavelengths taken from (A). A break point in the absorbance is reached at ~18-20 Cu(I) equivalents. Experiments were performed at 20 $^{\circ}$ C in 10 mM MOPS pH 7.5, 150 mM NaCl.

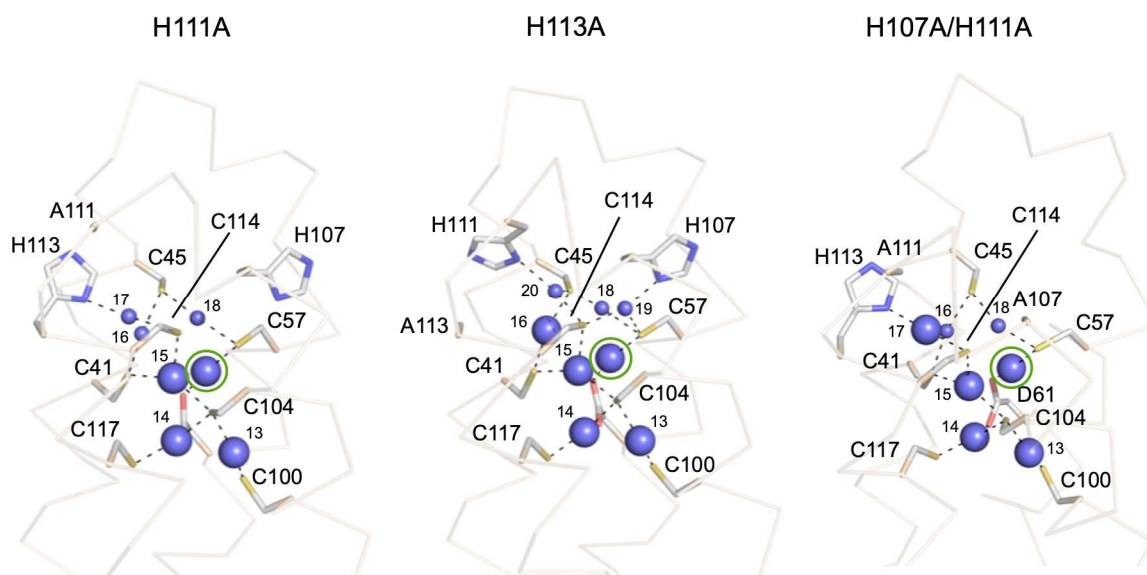


Figure 8: X-ray structures of the fully Cu(I)-loaded *S/Csp3* His variants. Close-up of the coordination chemistries of the Cu(I) ions (blue spheres) in the outer core with coordinate bonds indicated by dashed lines. The smaller spheres indicate partial occupancy, based on the anomalous electron-density peaks (Fig. S2) and the green circles indicate the location of non-cognate sites filled by Cu(I) ions.

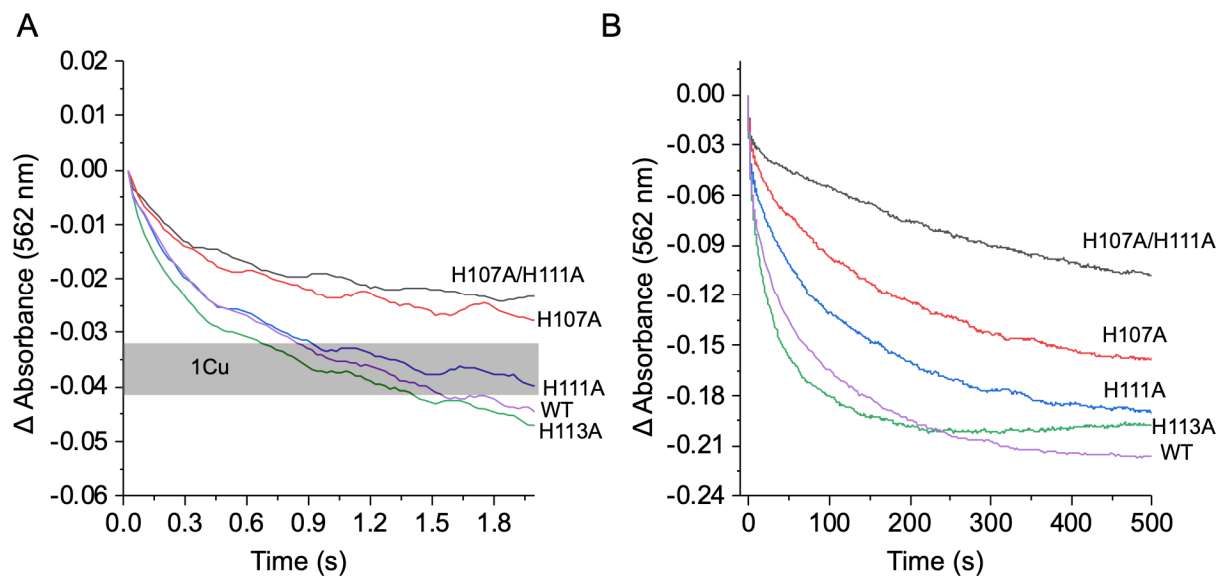


Figure 9: Kinetics of Cu(I) loading to the *S/Csp3* His variants from the $[\text{Cu}(\text{BCA})_2]^{3-}$ complex. A) and B) stopped-flow reaction time-courses monitored at 562 nm on mixing *S/Csp3* ($4.5 \mu\text{M}$) and the His variants ($5.5\text{-}5.8 \mu\text{M}$) with $50 \mu\text{M}$ $[\text{Cu}(\text{BCA})_2]^{3-}$ complex revealing an initial fast phase A) followed by slower phases B). Shaded area in (A) indicates the expected absorbance changes for removal of one Cu(I) equivalents from the $[\text{Cu}(\text{BCA})_2]^{3-}$ complex based on the variation of protein concentrations used. Experiments were performed at $20 \text{ }^\circ\text{C}$ in 10 mM MOPS pH 7.5, 150 mM NaCl.

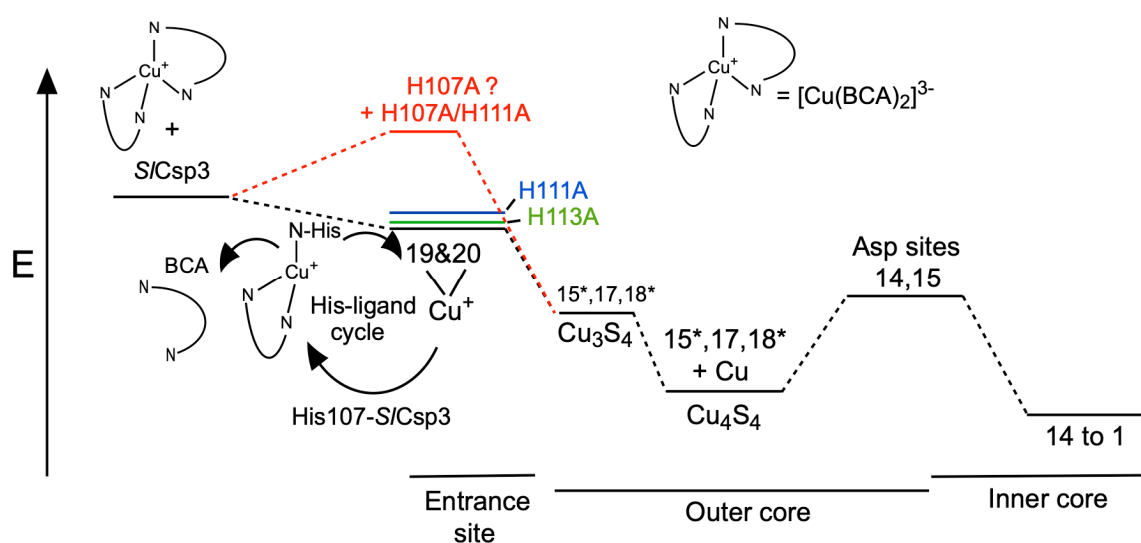


Figure 10: Scheme to illustrate Cu(I)-loading from the $[\text{Cu}(\text{BCA})_2]^{3-}$ complex to the Cu(I) sites in *S/Csp3*. The relative stabilities of the sites are depicted relative to an arbitrary energy scale. The extent of loading of Cu(I) is in accordance with the thermodynamic stabilities of the sites, whilst the kinetics of loading are controlled by ligand-exchange mechanisms between adjacent sites. See main text for details.